Since January 2020 Elsevier has created a COVID-19 resource centre with free information in English and Mandarin on the novel coronavirus COVID-19. The COVID-19 resource centre is hosted on Elsevier Connect, the company's public news and information website.

Biochimica et Biophysica Acta 1858 (2016) 2671–2680

Contents lists available at ScienceDirect

Biochimica et Biophysica Acta

journal homepage: www.elsevier.com/locate/bbamem

Structure and interaction with lipid membrane models of Semliki Forest virus fusion peptide

A. Agopian, M. Quetin, S. Castano *

CBMN-UMR 5248 CNRS, Université de Bordeaux, IPB, Allée Geoffroy Saint Hilaire, 33600 Pessac, France

ARTICLE INFO

Article history:
Received 22 March 2016
Received in revised form 21 June 2016
Accepted 12 July 2016
Available online 15 July 2016

Keywords:
SFV fusion peptide
Lipid/peptide interaction
Secondary structure
Viral fusion mechanism
IR spectroscopy
Ellipsometry

ABSTRACT

Semliki Forest virus (SFV) is a well-characterized alphavirus that infects cells via endocytosis and an acid-triggered fusion step using class II fusion proteins. Membrane fusion is mediated by the viral spike protein, a heterotrimer of two transmembrane subunits, E1 and E2, and a peripheral protein, E3. Sequence analysis of the E1 ectodomain of a number of alphaviruses demonstrated the presence of a highly conserved hydrophobic domain on the E1 ectodomain. This sequence was proposed to be the fusion peptide of SFV and is believed to be the domain of E1 that interacts with the target membrane and triggers fusion. Here, we investigate the structure and the interaction with lipid membrane models of $_{76}$YQCKVYTGVYPFMWGGAYCFC$_{96}$ sequence from SFV, named SFV21, using optical method (ellipsometry) and vibrational spectroscopiy approaches (Polarization Modulation infra-Red Reflection Absorption Spectroscopy, PMIRRAS, and polarized ATR-FTIR). We demonstrate a structural flexibility of SFV21 sequence whether the lateral pressure and the lipid environment. In a lipid environment that mimics eukaryotic cell membranes, a conformational transition from an α-helix to a β-sheet is induced in the presence of lipid by increasing the peptide to lipid ratio, which leads to important perturbations in the membrane organisation.

1. Introduction

Enveloped viruses must carry out a membrane fusion reaction between the virus and cellular membranes in order to infect the host cell. This fusion event is driven by viral fusion proteins present at the extracellular surface of the virions.

Virus membrane fusion proteins have been grouped into three classes based on shared structural features. The class I fusion proteins are characterized by a post-transductionnal cleavage which produces an amino-terminal fusion peptide as observed in orthomyxoviruses, paramyxoviruses, filoviruses, coronaviruses and retroviruses. The fusogenic structural transition leads to a trimeric assembly of α-helical coiled coil hairpins in the post fusion state. The class II contains fusion proteins of alphaviruses and flaviviruses. Conversely to class I proteins, they are not cleaved after synthesis and the fusion peptide is internal. They are found to be trimers of hairpins composed of β-sheets in the post fusion state. The class III contains fusion proteins of vesicular stomatitis virus (VSV), herpes simplex virus, and baculovirus, and shares structural features of both class I and class II (for review see references [1–5]).

These fusion proteins play a key role in the fusion process undergoing a large conformationnal change [1,2,4,6–8]. These conformational changes are triggered either by the interaction of the proteins with specific cell receptors or after cellular internalization, through the receptor mediated uptake by the endocytic pathway, when the acidic condition of the endosome activates the fusion protein [9,10]. However, while their structural features differ, all virus fusion proteins whose post-fusion structures have been defined mediate fusion through a common mechanism. Conformational changes allow the exposure of a region of the virus fusion protein that inserts directly into the viral and/or cell membranes to lead to their destabilization. These regions are named "fusion peptides" (FP) and are generally N-terminal or internal regions of 16 to 36 residues that are relatively hydrophobic in nature and are highly conserved within virus families [6].

Due to their important role in fusion process, numerous studies were carried out on FP to investigate membrane-associated structures and processes functioning in viral fusion [11]. If class I FPs were intensively studied (HIV [12–18], Influenza [19–22], SARS [23,24], Ebola [25–27], Paramyxovirus [28,29], it is noteworthy that similar studies of the FPs from class II fusion proteins are much more limited. One can mention a recent structural study on the FP of the Dengue virus which belongs to the flavivirus family [30] and one about the putative FP of Chikungunya virus which belongs to the alphavirus family [31], both performed by NMR in DPC micelles.

Abbreviations: DMPC, dimirystoyl-phosphatidylcholine; DMPG, dimirystoyl-phosphatidylglycerol; DMPE, dimirystoyl-phosphatidylethanolamine; PS, phosphatidylserine; PMIRRAS, polarization modulation infra-red reflection absorption spectroscopy; ATR, attenuated total reflexion spectroscopy; BAM, Brewster angle microscopy; Ri, lipid to peptide ratio.

* Corresponding author at: CBMN/University Bordeaux, Allée Geoffroy Saint Hilaire, F-33600 Pessac, France.
E-mail address: s.castano@cbmn.u-bordeaux.fr (S. Castano).

http://dx.doi.org/10.1016/j.bbamem.2016.07.003
0005-2736/

In the present study, we will focus on FP of the Semliki Forest virus. Semliki Forest virus (SFV) is a well-characterized alphavirus that infects cells via endocytosis and an acid-triggered fusion step using class II fusion proteins and whose fusion is characterized by a striking requirement of cholesterol in the target membrane (for review, see reference [3]). Membrane fusion is then mediated by the viral spike protein, a heterotrimer of two transmembrane subunits, E1 and E2, and a peripheral protein, E3. The pre- and post-fusion structures of the SFV E1 protein have been determined [32–34]. Sequence analysis of the E1 ectodomain of a number of alphaviruses demonstrated the presence of a highly conserved hydrophobic domain on the E1 ectodomain that lies ~80 residues from the N terminus, between amino acids 79 and 97. This sequence was originally proposed to be the fusion peptide of SFV and is believed to be the domain of E1 that interacts with the target membrane and triggers fusion [35–38]. Here, we propose to characterize the structure and the interaction with lipid membrane models of $_{76}$YQCKVYTGVYPFMWGGAYCFC$_{96}$ sequence from SFV, named SFV21, using an optical method (ellipsometry) and vibrational spectroscopy (PMIRRAS and polarized ATR-FTIR).

2. Materials and methods

2.1. Lipids and peptide

Lipids (dimirystoyl-phosphatidylcholine (DMPC), dimirystoyl-phosphatidylglycerol (DMPG), dimirystoyl-phosphatidylethanolamine (DMPE) and cholesterol) were purchased from Sigma. SFV21 peptide: YQCKVYTGVYPFMWGGAYCFC was purchased from GenScript (Piscataway, USA). SFV21 was solubilized in hexafluoroisopropanol (HFIP) from Sigma at micromolar concentrations. Peptide concentrations were calculated from the absorbance at 280 nm using a molar extinction coefficient ε_{280} of 11,200 $M^{-1}\cdot cm^{-1}$. The molar extinction coefficient of the peptide has been determined using the formula $\varepsilon_{280nm} = 5600 \times n_W + 1400 \times n_Y$ which takes into account the individual extinction coefficient of the amino acids W and Y. A Raman spectrum of a dried film of SFV21 after incubation in buffer (Supplementary data S1) was performed to insure that the three cysteins in the sequence remain non oxydized in the experimental conditions used (no band characteristic of S-S bond around 520–540 cm^{-1}, only a band characteristic of S—H bond in the 2500–2600 cm^{-1} region).

2.2. Film formation and surface pressure measurements

Monolayer experiments were performed on a computer-controlled Langmuir film balance (Nima Technology, Coventry, England). The rectangular trough and the barrier were made of Teflon. The surface pressure (π) was measured by the Wilhelmy method using a filter paper plate. The trough was filled with a saline solution (150 mM NaCl, pH 5.6) using ultra pure water (MilliQ, Millipore). The experiments were carried out at 22 ± 2 °C. Pure peptide films were obtained by spreading of few μl of HFIP peptide stock solutions at the air/water interface. The mixed lipids/peptides at the defined lipid to peptide ratio, Ri were obtained by co-spreading of the lipid/peptide mixture at the water surface. The monolayer lipid composition used was DMPC:DMPG:Cholesterol:DMPE (6:2:5:3). After ~15 min of stabilization, the film was slowly compressed up to 40 $mN\cdot m^{-1}$ and decompressed at the same rate speed than during the compression (8 $Å^2\cdot molecule^{-1}\cdot min^{-1}$).

2.3. PMIRRAS spectroscopy

PMIRRAS spectra were recorded on a Nicolet Nexus 870 spectrometer equipped with a photovoltaic HgCdTe detector cooled at 77 K. Spectra were obtained by performing 800 scans at a resolution of 8 cm^{-1}. Briefly, PMIRRAS combines FT-IR reflection spectroscopy with fast polarization modulation of the incident beam between parallel (p) and perpendicular (s) polarizations. The differential reflectivity spectrum is obtained using a two-channel processing signal. To remove the contribution of liquid water absorption and the dependence on Bessel functions, the monolayer spectra are divided by that of the subphase. With an incidence angle of 75°, transition moments preferentially oriented in the plane of the interface give intense and upward oriented bands, while perpendicular ones give weaker and downward oriented bands [39].

2.4. ATR spectroscopy of SFV21 in bulk solid state and inserted in a lipid bilayer

For bulk solid spectra, a film of SFV21 was obtained by evaporation of the peptide solution in HFIP on a germanium ATR crystal.

For experiments in lipid bilayer, small unilamellar vesicles (SUV) composed of DMPC:DMPG:Cholesterol:DMPE (6:2:5:3) were prepared alone or mixed with the fusion peptide at a defined molar ratio, Ri. For pure lipid SUVs, lipids were first dissolved in chloroform and mixed at the desired ratio. The solvent was then evaporated giving a lipid film. SUV were then prepared by tip sonication after direct hydration of the lipid film with a solution of D_2O containing 150 mM NaCl. For the preparation of the SUVs containing the mixed fusion peptide/lipids, the fusion peptide powder was first dissolved in HFIP then mixed with the lipids in chloroform at the desired ratio. Solvents were evaporated before hydration by D_2O and tip sonication for SUV formation. SUV were then burst on a germanium ATR crystal to form a single bilayer whose deposition is controlled by the measurement of the absolute IR intensity [12]. The experiments were carried out at 22 ± 2 °C.

ATR spectra were recorded on a Nicolet 6700 spectrometer Thermo Scientific equipped with a MCT detector cooled at 77 K. Since ATR spectroscopy is sensitive to the orientation of the structures [40–42], spectra were recorded with parallel (p) and perpendicular (s) polarizations of the incident light with respect to the ATR plate. 400 scans were recorded at a resolution of 8 cm^{-1}. All the orientation information is then contained in the dichroïc ratio $R_{ATR} = Ap/As$, where Ai respectively represents the absorbance of the considered band at p or s polarization of the incident light.

The determination of the position of the band maximum was obtained by second-derivative method and the decomposition of the amide I band in single components characteristic of each secondary structure has been calculated using Omnic or GRAMS V.5 software (Galactic Software).

2.5. Ellipsometric measurements

The morphology of pure peptides or mixed lipids with the peptides were observed at the air/water interface using an ellipsometer iElli2000 microscope (NFT, Göttingen, Germany) mounted on a Langmuir trough. The microscope was equipped with doubled frequency Nd:Yag laser (532 nm, 50 mW), a polarizer, a compensator, an analyzer and a CCD camera. The spatial resolution of the pictures with the 10x magnification lens was about 2 μm and the image size 600 × 450 μm. For ellipsometric measurements, the imaging ellipsometer works at an incidence angle close to the Brewster angle (54.6°). It operates using the principle of a classical null ellipsometer [43].

The ellipsometric angles (Δ, Ψ) are determined from polarizer and analyzer azimuths at extinction; Δ and Ψ are related to the optical properties of the sample. In ultra-thin film conditions, Δ is proportional to the film thickness. The comparison of the experimental data with a computerized optical model included in the ellipsometer software allowed to provide an estimation of the film thickness when a value of refractive index can be obtained. Since it is difficult to determine an experimental refractive index value, we choose 1,50 for the SFV21 peptides as it was used in a previous work concerning the fusion peptide FP23 of HIV and EBO17 and EBO 24 of Ebola [12,27]. Indeed, in the literature, variations between 1,45 [44] and 1,53 [45,46] can be encountered

for protein and peptide depending on the amount of water taken into account. Concerning lipids, anisotropic refractive indices between 1.44 [47] and 1.50 [48] were reported for DMPC in the literature. Therefore, we use an intermediate value of 1,46 to perform thickness estimations [12,27].

3. Results

3.1.1. Structure of SFV21 in the bulk solid state by ATR spectroscopy

ATR FT-IR absorption spectrum of SFV21 in the bulk solid state displays an intense asymmetric amide I band centered around 1625 cm^{-1} (Fig. 1). The amide I region was analyzed and the secondary structure content was evaluated from the analysis of the amide I band shape and curve fitting [40]. The decomposition of the spectrum shows that the main band around 1625 cm^{-1} is well fitted by two components at 1628 and 1615 cm^{-1}. Associated with another weak contribution around 1694 cm^{-1}, these three bands are characteristic of antiparallel β-sheets which contribute for 49.0% of the secondary structure. Another contribution at 1656 cm^{-1} can be attributed to α-helix and represents 31.5% of the structure. Two other minor contributions are observed at 1644 cm^{-1} and 1677 cm^{-1}, they are assigned respectively to random structure and β-turn and contribute for 6.3% and 13.2% respectively [40,41,49,50]. The amide II mode absorbs around 1520 cm^{-1}.

3.2. Morphological and structural study of the SFV21 at the air/water interface

The Brewster angle microscope (BAM) images of the pure SFV21 layer at increasing surface pressures from 2 to 20 mN/m (Fig. 2) displays a progressive increase of the averaged normalized grey level until 20 mN/m. Every picture shows a stable homogeneous surface of the peptide layer even at low pressures such as 2 mN/m and the peptide film appears brighter during compression. The thickness of the layer was estimated by ellipsometry using a constant refractive index of 1.50 for the peptide (cf Materials and methods). As the peptide film is compressed, estimated thickness increases from 21 ± 1 Å (Δ = 347.40°, Ψ = 2.39°) at 2 mN/m to 24 ± 1 Å (Δ = 345.23°, Ψ = 2.40°) at 12 mN/m and 26 ± 1 Å (Δ = 343.29°, Ψ = 2.40°) at 20 mN/m.

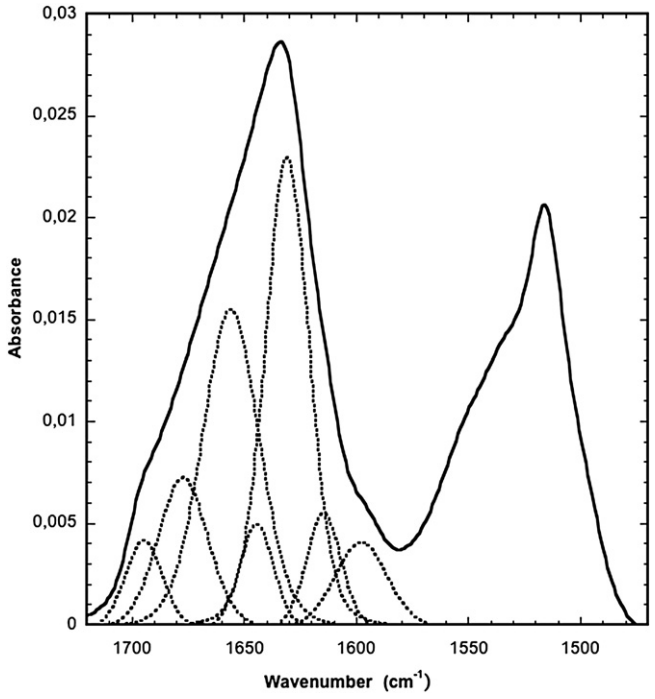

Fig. 1. ATR FT-IR spectrum of SFV21 in bulk state (solid line) and components obtained by decomposition (dotted line).

The PMIRRAS spectra at the air/water interface of the SFV21 peptide film during compression from 1 to 20 mN/m displayed well resolved amide I bands between 1600 and 1700 cm^{-1} and amide II bands centered around 1530 cm^{-1} (Fig. 3). Whatever the surface pressure from 2 to 20 mN/m, the main amide I band is centered around 1626 cm^{-1} with another contribution around 1695 cm^{-1} reflecting a main content of antiparallel β-sheets. Shoulders and secondary derivative (not shown) display also contributions around 1645 cm^{-1}, 1655 cm^{-1} and 1670 cm^{-1} respectively characteristic of random, α-helical and β-turn structures [41,49,50]. During compression of the peptide film (up to 20 mN/m), since their contributions remain positive, one can assume that antiparallel β-sheets are mainly oriented flat on the air/water interface plane [51,52] whatever the lateral pressure. Simultaneously, the Amide I/Amide II ratio decreases from 1.9 to 1.4 during the compression from 2 to 12 mN/m, and remains constant around 1.4 at 20 mN/m. Due to the specificity of the PMIRRAS selection rules, this change in the amide I/amide II ratio could be attributed both to a change in the orientation of one or more of the minor structural components or to a concomitant change in their proportion.

This experiment suggests that SFV21 remains mainly folded into antiparallel β-sheets laying flat at the air/water interface during compression and decompression, and that the contribution of other minor structures can slightly change both in proportion and orientation versus lateral pressure changes.

3.3. Morphological and structural study of SFV21 inserted into a lipid monolayer

To investigate the changes in morphology induced by SFV21 upon interaction with the DMPC:DMPG:cholesterol:DMPE monolayer at the molar ratio 6:2:5:3, we first studied the morphology of the lipid alone in the surface pressure range from 5 to 30 mN/m. Such a complex lipid composition was used to reflect the variety of lipids present in eukaryotic cell membranes [53]. PC and PE polar heads and cholesterol are main components in this type of membrane. We replaced the negatively charged PS polar headgroup generally encountered in natural membranes by PG in our model since the asymmetric stretching band of the PS carboxylate group overlaps with the amide I band of proteins and thus interferes with IR measurements. We choose myristoyl fatty acid chains for their stability at the air water interface and to avoid oxydation processes like encountered with C18:1 like DOPC at the interface. This composition was also chosen to allow comparison with the FP23 fusion peptide of HIV and the Ebola fusion peptide previously studied in these conditions with the same techniques [12,27].

BAM pictures (Fig. 4, first row micrographs) show that the surface is homogeneous whatever the surface pressure during compression and decompression. Such an observation is surprising since the monolayer contains DMPE and cholesterol which display high phase transition temperatures (>49 °C) compared to DMPC and DMPG (23 °C), then one can expect to observe segregation of lipids in the monolayer. Taking into account the large content of cholesterol in the monolayer, the observation of such a homogeneous film can probably be explained by attractive interactions between the different phospholipids and cholesterol as previously reported [54]. Ellipsometric measurements and thickness estimations using a refractive index of 1.46 for the lipids (cf Materials and methods) leads to 16 ± 1 Å (Δ = 350.93°, Ψ = 2.39°) for the thickness of the lipid monolayer at 5 mN/m, 17 ± 1 Å (Δ = 350.75°, Ψ = 2.40°) at 15 mN/m and 18 ± 1 Å (Δ = 349.88°, Ψ = 2.39°) at 30 mN/m.

BAM pictures of SFV21 inserted into a lipid monolayer are recorded after co-deposition at the air/water interface of a peptide/lipid (DMPC:DMPG:Cholesterol:DMPE 6:2:5:3) mixture at a defined lipid to peptide ratio, Ri = 75 or Ri = 20. When SFV21 is inserted into the

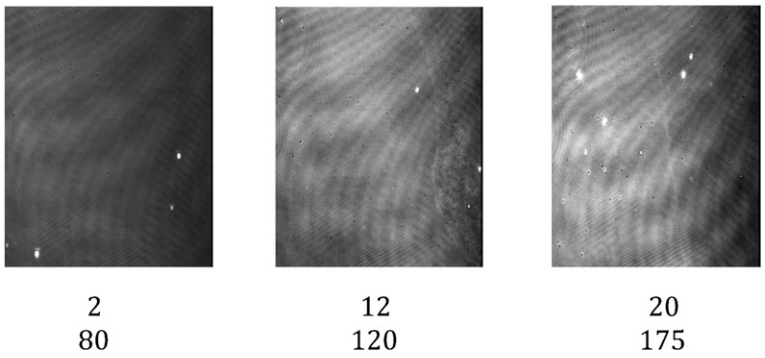

Fig. 2. BAM images of SFV21 alone at the air/water interface. Exposition time for each image was fixed at 1/50 s. Sub-phase: saline solution, 150 mN NaCl, pH 5.6. GL: grey level.

lipid monolayer at low surface pressure (5 mN/m), whatever the Ri, an homogeneous surface is observed with gray levels and ellipsometric measurements comparable to what is observed for lipids alone. For higher lateral pressures, important changes in the morphology of the layer are observed compared to the lipid alone (Fig. 4). Whatever the pressure and the lipid/peptide ratio Ri (75 or 20) heterogeneous surfaces are observed which are characterized by a brighter network/phase in a surrounding less dense phase (dark background). The brightness of the denser phase increases with lateral pressure from 15 to 30 mN/m but is comparable whatever the SFV21 content (Ri from 75 to 20). Estimations performed using ellipsometric measurements lead to thicknesses around 19 ± 1 Å at Π = 15 mN/m and 30 ± 2 Å at Π = 30 mN/m for both Ri (75 and 20). For the less dense phase, whatever the Ri (75 or 20) and the surface pressure (15 to 30 mN/m), thicknesses are highly comparable to what was obtained for the lipid alone (17 ± 1 Å at 15 mN/m and 19 ± 1 Å at 30 mN/m). The decompression down to 15 mN/m shows a reversible behaviour both in morphology and thicknesses and further decompression down to 5 mN/m (not shown) leads back to a homogenization of the surface.

PMIRRAS spectra of SFV21 inserted into a DMPC:DMPG:cholesterol:DMPE (6:2:5:3) lipid monolayer at Ri = 20 and 75 were recorded as previously described. Since the results obtained for both Ri are very comparable, only the spectra at Ri = 20 are presented in Fig. 5. The mixed monolayer was compressed from 5 to 40 mN/m then decompressed down to 5 mN/m. PMIRRAS spectra were recorded at different surface pressures (Fig. 5A). Every spectrum shows a band centered around 1732 cm^{-1} characteristics of the ν(C═O) ester stretching vibration [55]. The δ (CH_2) bending vibration of acyl chains around 1465 cm^{-1} can also be observed. Whatever the lateral pressure, in the amide I region, the main contribution around 1627 cm^{-1} is characteristic of β-sheets. A shoulder around 1650 cm^{-1}, characteristic of α-helix, is present whatever the lateral pressure and increases with compression. The weak amide II contribution whatever the spectrum shows that the structures are mainly laying flat at the interface and that the orientation does not significantly changes with lateral pressure increase [56]. To have a better insight on the secondary structure, the difference spectrum between lipids and absence and presence of SFV21 at comparable lateral pressure was calculated (Fig. 5B). For this, separate PMIRRAS measurements with monolayers of the pure lipids were registered at the same surface pressure and we assume that these spectra can be used for the subtraction. The data clearly show that the two main secondary structure contributions are due to the 1650 cm^{-1} and 1627 cm^{-1} bands, and that their respective proportions vary depending on the applied lateral pressure. One can observe that the position of the alpha helical and beta sheet components of the amide I band in Fig. 5A remains unchanged in all spectra whereas some differences in position and shape of some of the amide I bands appear in Fig. 5B. This can mainly be explained by the fact that this region of the spectrum (broad negative dip around 1650 cm^{-1} associated with the deformation vibrational mode of liquid water [57]) is sensitive to the interface coverage, then small differences in the pure lipid film organisation compared to the mixed SFV21/lipid film can lead to small distortions. To minimize these effects and assuming that the main contributions to the secondary structures are due to these bands and that the orientation does not change significantly, the area of the band was estimated and the respective proportion of both secondary structures calculated using three independent experiments. The results are summarized in Table 1 for Ri = 20 and Ri = 75. The values show that whatever the Ri, at low lateral pressure, the β-sheet structure is largely predominant. The β-sheet proportion decreases with lateral pressure increase while the α-helix proportion increases. The α-helical proportion becomes predominant from 15 mN/m (55,5%) at Ri = 75, while it slowly increases up to 48% for 35mN/m at Ri = 20. These results show a progressive secondary structure transition from β-sheet to α-helix induced by compression of the monolayer, the behaviour is more pronounced for the higher Ri (75), then the lower SFV21 content. This behaviour demonstrates a structural flexibility of the SFV21 sequence and shows that the conformation is both sensitive to lateral pressure and to the presence of lipids. During decompression, the transition is not reversible since the α-helix predominates compared to the β-sheet whatever the RI.

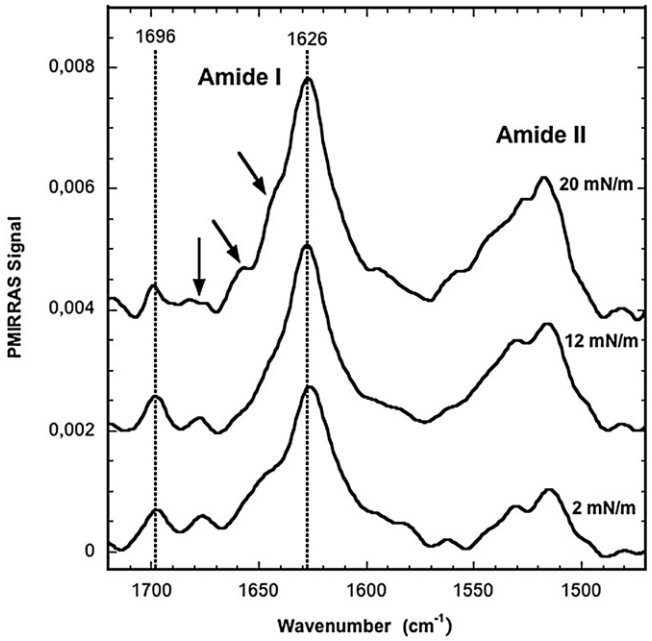

Fig. 3. PMIRRAS spectra of SFV21 alone at the air/water interface during compression.

To estimate the effect of the SFV21 incorporation on the lipid chain organization, the position of the band corresponding to asymmetric stretching modes of the methylene groups, $\nu_{as}(CH_2)$, was measured

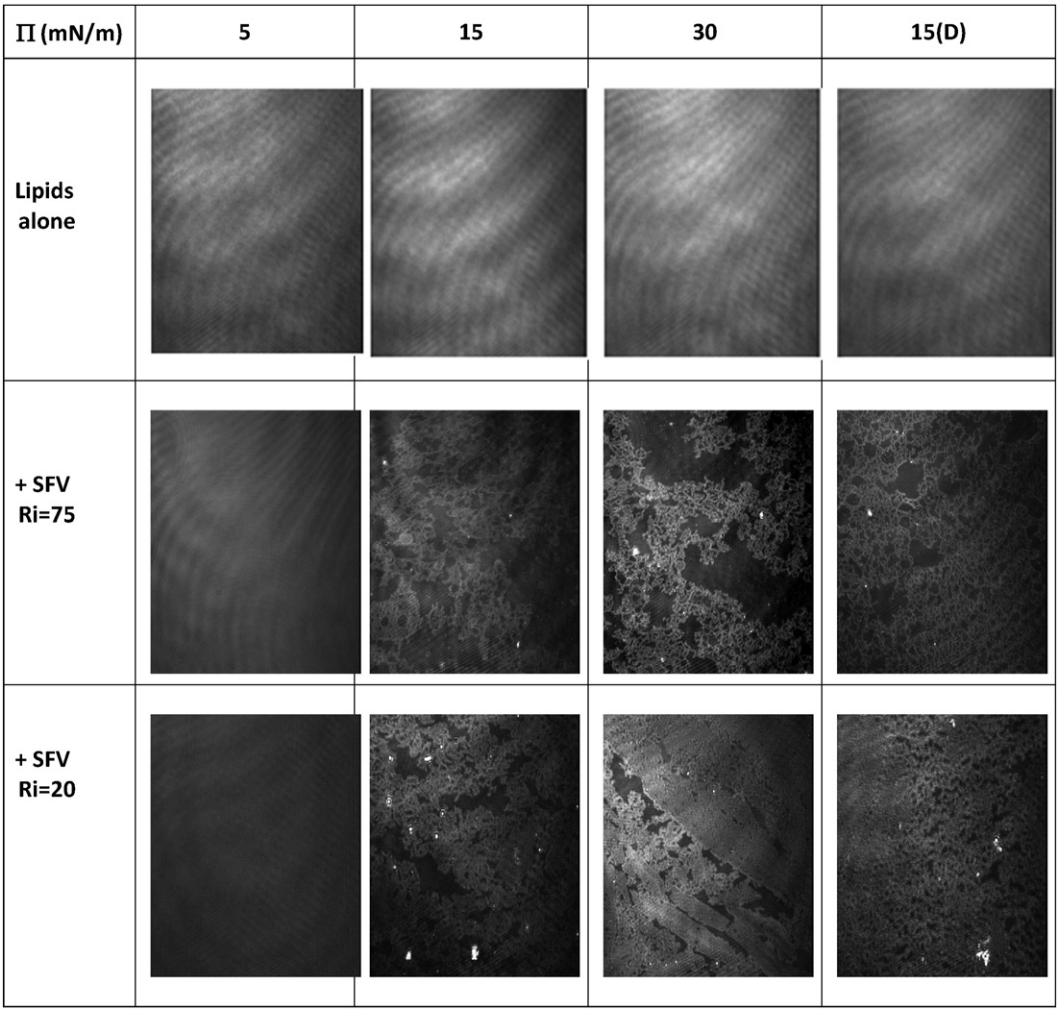

Fig. 4. BAM images of a lipid monolayer composed of DMPC:DMPG:cholesterol:DMPE 6:2:5:3 (first line), mixed DMPC:DMPG:cholesterol:DMPE (6:2:5:3)/ SFV21 at Ri = 75 (second line) and Ri = 20 (third line). Exposition time for each image was fixed at 1/50 s. Subphase: saline solution, 150 mN NaCl, pH 5.6.

(Table 2) since it is sensitive to the lipid chain order [58–60]. We then observe a slight decrease in the wavenumber of the $\nu_{as}(CH_2)$ when the lateral pressure increases from 5 to 35 mM/m, due to the progressive organization of the lipid chains during compression. It is then interesting to notice that at low lateral pressures (<15 mN/m), there is no noticeable difference in wavenumber of the $\nu_{as}(CH_2)$ in absence or presence of SFV21, while at higher pressures (>25 mN/m), the wavenumber of $\nu_{as}(CH_2)$ is higher in presence of SFV21 than for the lipid monolayer alone. This shows a more important disorder in the lipid chain packing in the monolayer due to the SFV21 incorporation. The higher the SFV21 concentration (the lower the Ri), the more important the disorder.

3.4. Study of SFV21 inserted into lipid bilayers

We further investigated the behaviour of SFV21 inserted into a single supported lipid bilayer made of the same lipid mixture DMPC:DMPG:cholesterol:DMPE (6:2:5:3). We hence performed polarized ATR experiments in order to analyze the structure of the fusion peptide in such membrane models as well as perturbations induced by the peptide on the organization of the lipids.

The pure or mixed SF21/lipid bilayers adsorbed on a germanium ATR crystal were obtained by spontaneous fusion of small unilamellar vesicles (SUV) of pure lipid or mixed SF21/lipid at the defined Ri as described in the Materials and methods section. Fig. 6 displays the ATR spectra obtained in the 1800–1500 cm^{-1} region. The band around 1735 cm^{-1} corresponds to the $\nu(C=O)$ ester of the lipids while the 1700–1600 cm^{-1} domain corresponds to the amide I. The amide I region was analyzed and the secondary structure content was evaluated from the analysis of the amide I band shape and curve fitting (Supplementary data S2) [39]. The 1685 ± 1 cm^{-1}, 1632 ± 1 cm^{-1} and 1624 ± 1 cm^{-1} bands were assigned to β-sheets, the 1664 cm^{-1} and 1653 ± 1 cm^{-1} bands to α-helices, the 1642 ± 2 cm^{-1} band to random structures and the 1675 ± 2 cm^{-1} band to β-turns. The results, presented in Table 3, show that the predominant structures are the α-helices and the β-sheets. There is a progressive interconversion from the predominant α-helices (41,0% at Ri = 150) to the β-sheets (37,2% at Ri = 20) with peptide concentration. The other structures, β-turns and random, counts respectively for around 10% and 20% and their proportion remains constant whatever the Ri. Using the p- and s-polarized spectra, we then estimated the dichroïc ratio of the amide I band of the α-helix (1664/1653 cm^{-1}) and of the β-sheet (1632/1624 cm^{-1}) presented in Table 3. The evolution of R_{ATR} (amide I) for the α-helix from 1.44 (Ri = 150) up to values between 1.8 and 2.0 demonstrates a progressive reorientation of the α-helix tilt angle from around 70° to 0–20¨compared to the interface normal [12]. This means that when diluted in the lipids, the helix is mainly laying flat on the membrane while its becomes perpendicular to the plane of the bilayer at higher concentration. Concerning the β-sheet, the weak variation of R_{ATR} (amide I) allows to estimate a tilt angle around 35° relative to the membrane plane, this orientation does not significantly depends on the peptide concentration [12].

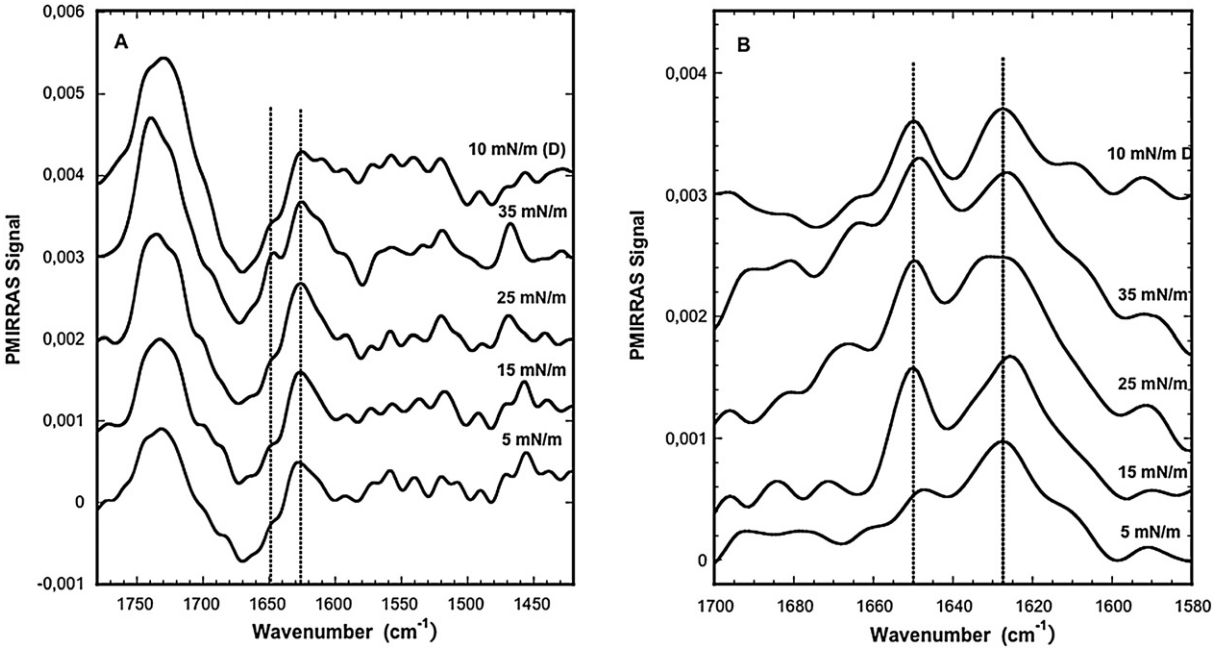

Fig. 5. A) PMIRRAS spectra of SFV21 inserted into a lipid monolayer of DMPC:DMPG:cholesterol:DMPE (6:2:5:3) at Ri = 20 during compression and decompression (d). B) Substracted PMIRRAS spectra of SFV21 inserted into a lipid monolayer of DMPC:DMPG:cholesterol:DMPE (6:2:5:3) at Ri = 20 during compression and decompression (d). Subphase: saline solution, 150 mN NaCl, pH 5.6.

To investigate the consequence of SFV21 bilayer incorporation on the organization of the lipid acyl chains in the bilayer, the shift of the bands corresponding to asymmetric and symmetric stretching modes of the methylene groups, $\nu_s(CH_2)$ and $\nu_{as}(CH_2)$, respectively, were measured (Table 4). Indeed, the wavenumbers of these bands are known to be sensitive to changes in the configuration of the acyl chains, in chain mobility and packing [53–56]. The $\nu_s(CH_2)$ and $\nu_{as}(CH_2)$ of 2851.7 and 2920.7 cm^{-1} respectively for the bilayer alone are characteristic of quite well ordered acyl chains, which is consistent with a bilayer composed of phospholipids with phase transition temperature higher than 23 °C. When SFV21 is added to the bilayer, there is an increase up to 1.8 ± 0.3 cm^{-1} at Ri = 20 in the wavenumbers of the $\nu_s(CH_2)$ and $\nu_{as}(CH_2)$ which indicates a decrease in chain order due to SFV21 peptide incorporation (Table 4). This is confirmed by the evolution of the dichroic ratio (R_{ATR}) of the $\nu_s(CH_2)$ band of lipid chains which was measured on the polarized ATR spectra (Table 4). Indeed, since the transition moment for the $\nu_s(CH_2)$ lies perpendicular to the chain axis, the introduction of order or disorder alters the direction of the main chain with respect to the normal of the ATR crystal. The dichroic ratio is then expected to provide a sensitive and quantitative indicator of acyl chain order by estimating the average C—C—C angle of the lipid carbon chains with the normal to the interface [12,27]. Here, the R_{ATR} increases when SFV21 interacts with the lipids, compared to the lipid alone (Table 4). This corresponds to a reorientation of the lipid chains from approximately 45° defined to the membrane normal to 60–65° in presence of SFV21 at Ri = 150 and 75. A R_{ATR} value of 1,93 obtained at Ri = 20 is characteristic of an important disorder of the bilayer, close to the isotropy [12]. Conversely, the dichroïc ratio of the ν(C = O) ester band of the lipids increases from 1.67 for the lipid alone to around 2.00 in the presence of SFV21 at Ri = 75 and 20 which is characteristic of an important increase of disorder. Altogether, this experiment is showing SFV21 insertion leads to disorder increase in both the acyl chains and the glycerol region of the lipids, but the glycerol region is sensitive at higher Ri compared to the acyl chains.

Table 1
Estimation of α-helix and β-sheet relative proportions in SFV21 inserted into a lipid monolayer of DMPC:DMPG:cholesterol:DMPE (6:2:5:3) during compression and decompression (D) (±5%) obtained from subtracted PMIRRAS spectra.

Π (mN/m)	Ri = 20		Ri = 75	
	1650 cm^{-1} (α-helix)	1627 cm^{-1} (β-sheet)	1650 cm^{-1} (α-helix)	1627 cm^{-1} (β-sheet)
5	29,5	70,5	29,5	70,5
15	40,5	59,5	55,5	44,5
25	41,0	59,0	–	–
30	–	–	62,0	38,0
35	48,0	52,0	–	–
15 D	–	–	74,5	25,5
10 D	45,0	55,0	–	–

4. Discussion

4.1. Influence of environmental conditions on SFV21 conformation

The structural studies of SFV21 show a sensitivity of its conformation whether the conditions used. Indeed, for SFV21 in bulk state or alone at the air/water interface whatever the compression state, the main conformation is an antiparallel β-sheet. In presence of lipids (monolayer at air/water interface and bilayer), SFV21 undergoes a conformational change from α-helix to antiparallel β-sheet.

Two parameters play a role in the SFV21 structuration: the lateral pressure and the presence of lipids. At low lateral pressure at the air/water interface (with or without lipid), the main conformation of SFV21 is the antiparallel β-sheet. This structure may be favoured by the large surface available since β-sheets occupy a larger area at the

Table 2
Wavenumbers of ν_{as} (CH_2) of lipid chains in the monolayer in absence and in presence of SFV21 peptide at different lateral pressures during compression. Lipid composition: DMPC:DMPG:cholesterol:DMPE (6:2:5:3).

Π (mN/m)	Lipid monolayer	+ SFV21 Ri = 75	+ SFV21 Ri = 20
5	2922,0 ± 0,4	2921,9 ± 0,4	2921,8 ± 0,4
15	2921,2 ± 0,4	2921,4 ± 0,4	2921,9 ± 0,4
25	2919,5 ± 0,4	2921,4 ± 0,4	2921,4 ± 0,4
35	2919,5 ± 0,4	2920,1 ± 0,4	2921,4 ± 0,4

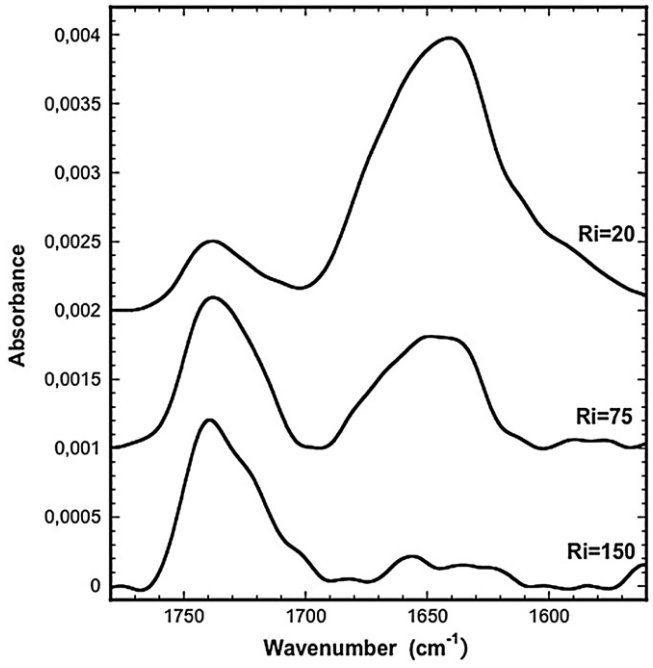

Fig. 6. ATR isotropic spectra of the amide I region of SFV21 inserted into a lipid bilayer DMPC:DMPG:cholesterol:DMPE (6:2:5:3) hydrated with D_2O and 150 mM NaCl, pH 5.6.

interface than α-helices and by the fact that the hydrophobicity of the air/water interface may favour changes in the hydrogen bonding interactions [61,62]. Increasing lateral pressure for pure SFV21 monolayer at the air water interface only leads to weak changes in the proportions and/or orientation of the minor structural components as shown by PMIRRAS spectra. The addition of lipids leads to a different structural behaviour of SFV21 by increasing lateral pressure of the mixed lipid/peptide monolayer with a progressive increase of the α-helix contribution. This phenomenon demonstrates a specific interaction of SFV21 with lipids which can modify the hydrogen bonding network. Such interactions are also prooved by the formation of aggregates at the air/water interface when SFV21 is inserted into the lipid monolayer, while no aggregates are observed both for the pure lipid and the pure SFV21 film (BAM microscopy and ellipsometry). In further studies it could then be interesting to investigate potential specific interactions of SFV21 fusion peptide with cholesterol which is present at high content in the membrane composition used (30% molar) since SFV alphavirus fusion with host cells is characterized by a striking requirement for cholesterol in the target membrane [3]. Cholesterol effect on

Table 3
Wavenumbers, secondary structure contents and dichroïc ratio for Amide I band for SFV21 in supported lipid bilayer at different lipid/peptide ratio Ri obtained by fit of the ATR-IR spectra in the amide I region. Lipid composition: DMPC:DMPG:cholesterol:DMPE (6:2:5:3).

	Secondary structure	Wavenumber (cm^{-1})	% (±1.0)	R_{ATR} (Amide I) (±0.05)
Ri = 150	β-Sheet	1624–1633–1685	28,7	1,55
	Random	1642	19,7	–
	α-Helix	1654–1663	43,0	1,44
	B-Turn	1677	8,6	–
Ri = 75	β-Sheet	1624–1633–1681	31,5	1,45
	Random	1643	21,2	–
	α-Helix	1653–1664	37,8	1,80
	β-Turn	1673	9,5	–
Ri = 20	β-Sheet	1617–1631–1685	37,2	1,50
	Random	1642	20,6	–
	α-Helix	1653–1664	33,1	2,05
	β-Turn	1675	9,1	–

Table 4
Wavenumbers and dichroïc ratio of ν_{as} (CH_2) and ν_s (CH_2) of lipid chains and dichroïc ratio of ν(C = O)) ester band around 1735 cm^{-1} in absence and in presence of SFV21 peptide. Lipid composition: DMPC:DMPG:cholesterol:DMPE (6:2:5:3).

	ν_{as} (CH_2) (cm^{-1})	ν_s (CH_2) (cm^{-1})	R_{ATR} ν_s (CH_2))	R_{ATR} (ν(C = O))
SUV alone	2920,7 ± 0,4	2851,7 ± 0,3	1,34 ± 0,05	1,67 ± 0,05
Ri = 150	2921,4 ± 0,4	2851,5 ± 0,3	1,73 ± 0,05	1,72 ± 0,05
Ri = 75	2922,2 ± 0,4	2852,3 ± 0,3	1,85 ± 0,05	2,03 ± 0,05
Ri = 20	2922,5 ± 0,4	2853,5 ± 0,3	1,93 ± 0,05	1,97 ± 0,05

membrane fusion has been extensively studied, and cholesterol demonstrated to be necessary for very different fusion processes as neuronal exocytosis [63] and viral entry. Indeed several recent studies on viruses as different as Influenza [64], Human or Feline Immunodeficiency Virus [65–68], Herpes Simplex virus [69] demonstrate the potential role of cholesterol or cholesterol-enriched domains (rafts) as possible platforms for the entry of viruses into cells.

It is also interesting to compare our results on SFV21 to these obtained for the putative fusion peptide VT18 of Chikungunya alphavirus using NMR spectroscopy in zwitterionic lipid environments [31]. VT18 is an 18 residue-long peptide which shares 13 residues with SFV21 (VYPFMWGGAYCFC). In the conditions used (DPC micelles at diluted lipid to peptide ratio around 250), authors do not observe significant contribution of α-helices as we observe in lipid bilayers in diluted conditions but rather extended or β-type conformations for most of the residues. Authors compare the NMR derived DPC bound structure of VT18 with that of the conformation deduced in the context of protein complexes (prefusion state) obtained by X-ray crystallography [70]. They show that the micelle-bound structure of the fusion peptide, VT18, markedly differs in terms of packing interactions of some aromatic residues compared to the the X-ray structure and conclude that the lipidic environment of DPC micelles led to a significant conformational reorganization of the aromatic residues in the fusion peptide. This result is in agreement with the observation that the conformation of fusion peptides is very sensitive to the lipid environment as well as the experimental conditions used. Concerning VT18, authors also observe that residues MWGG adopt a type I β-turn conformation with the N- and C-termini pointing in an antiparallel orientation. In our case, we show that in lipid bilayer environment, the proportions of random and β-turn structure remain rather constant whatever the Ri (≈20% and ≈9% respectively). It cannot be excluded that this relatively high but conserved proportion of random and β-turn could be due to this part of the sequence. One can also speculate that the presence of such a β-turn will result in a partial folding of SFV21 into intramolecular antiparallel β-sheet for the residues close to the turn, the structural plasticity resulting from the N- and C- terminal part of the sequence and from the 8 residues which are not present in the VT18 sequence.

It is then interesting to see that the conformational flexibility observed for SFV21 fusion peptide of class II is also shared by viral fusion peptide of class I (HIV1, paramyxovirus, Ebola [12–27]) and SNARE proteins involved in intracellular fusion process [71]. These similarities on structural properties shared by peptides or proteins involved in totally different fusion processes may play an important role in the fusion mechanism.

4.2. SFV21 interaction with model membranes

The present study shows that, whatever the lipid membrane model used, monolayer at lateral pressure close to "biological equivalent pressure" of a bilayer around 30–35 mN/m or lipid bilayer, the structural behaviour of SFV21 fusion peptide is comparable (Table 5). A conformational transition from an α-helix to a β-sheet is induced by a change in the peptide to lipid ratio in the membrane. At low concentration in lipids, SFV21 interacts with lipids mainly as α-helices. As the

Table 5
Relative percentage of α-helix of SFV21 inserted into lipid membrane models (mono- and bilayer) at different lipid/peptide ratios (Ri). Lipid composition: DMPC:DMPG:cholesterol:DMPE (6:2:5:3). Accuracy estimated to within ca ±5%.

α/(α + β) %	Lipid monolayer	Lipid bilayer
Ri = 150	–	60
Ri = 75	62	58
Ri = 20	48	47

local peptide concentration increases in the membrane, the proportion of α-helix drops off in favor of a mainly antiparallel β-sheet structure. The formation of antiparallel β-sheet structure is probably due to peptide self-assembling triggered by close peptide contacts induced by increasing their concentration (Fig. 7). This is confirmed by the aggregates which are observed in presence of SFV21 by BAM and ellipsometry. This concentration dependent effect on peptide conformation might be of biological relevance during the formation of the trimers of hairpins composed of β-sheets as seen in the post-fusion state of class II fusion proteins. Formation of fusion oligomers was already suggested for class I viruses like HIV to be linked to fusion activity for both envelope protein-mediated fusion and for liposome fusion mediated by fusion peptides [72,73]. For instance, in the case of the fusion peptide of the Sendaï virus [74], the peptide could self-assemble in its membrane-bound state, thus suggesting its role in assisting the assembly of the envelope protein of the virus.

This structural plasticity with formation of β-sheets as fusogenic conformation, may then promote membrane topological changes during fusion. Indeed, we observe by ATR spectroscopy that while the proportion of the β-sheets increases with the SFV21 concentration, the β-sheets remain tilted compared to the interface plane of the bilayer (35°), which lead to important disorder in the lipid chain organisation as observed by the increase of the R_{ATR} and of the wavenumber of bands characteristic of the stretching of the chain acyl groups. Conversely, while the proportion of α-helix decreases with SFV21 concentration increase, their orientation becomes perpendicular to the plane of the lipid bilayer, which may result in a weaker perturbation of the lipid chain organization but a destabilization of the lipid head groups [12]. It is also interesting to notice that we do not observe this orientationnal change with the monolayer lipid model. Such a difference may be due to the fact that a lipid monolayer does not match correctly the hydrophobic thickness of a membrane and does not allow a proper orientation of SFV21 α-helix which is then too long to match the hydrophobic part of the lipids. Therefore, even if the monolayer system allows the detection of the structural plasticity of SFV21, the lipid bilayer model seems to be more relevant in mimicking the biological membrane and the orientation of SFV21 in such a system will be more representative of the reality.

Such a process of lipid bilayer disorganization should be essential during membrane fusion processes by generating new lipid phases that are thought to be associated with initial steps of membrane fusion by increasing the negative curvature strain, favoring the formation of inverted phases [75,76].

To conclude, the present study shows the structural plasticity of SFV21 fusion peptide and demonstrates its ability to transit from a mainly α-helical structure to antiparallel β-sheets leading to a destabilization at large scale of the lipid membrane. Such a process is probably combined with concerted effects due to various domains of the viral fusion proteins, besides the fusion peptide, which could cooperate in destabilizing the apposing viral and plasma membranes. Our results show then the interest of this type of fundamental study to highlight some specific structural properties (flexibility, plasticity) shared by fusion peptides belonging to different fusion processes (viral fusion, intracellular fusion) which could play a key role in the fusion mechanism.

Transparency document

The Transparency document associated with this article can be found, in online version.

Acknowledgements

We acknowledge ANR-09-BLAN-0385-02 for its financial support.
We acknowledge Etienne Harté for registration of the Raman spectrum and Dr. Isabel Alves for its careful reading of the manuscript.

Appendix A. Supplementary data

Supplementary data to this article can be found online at http://dx.doi.org/10.1016/j.bbamem.2016.07.003.

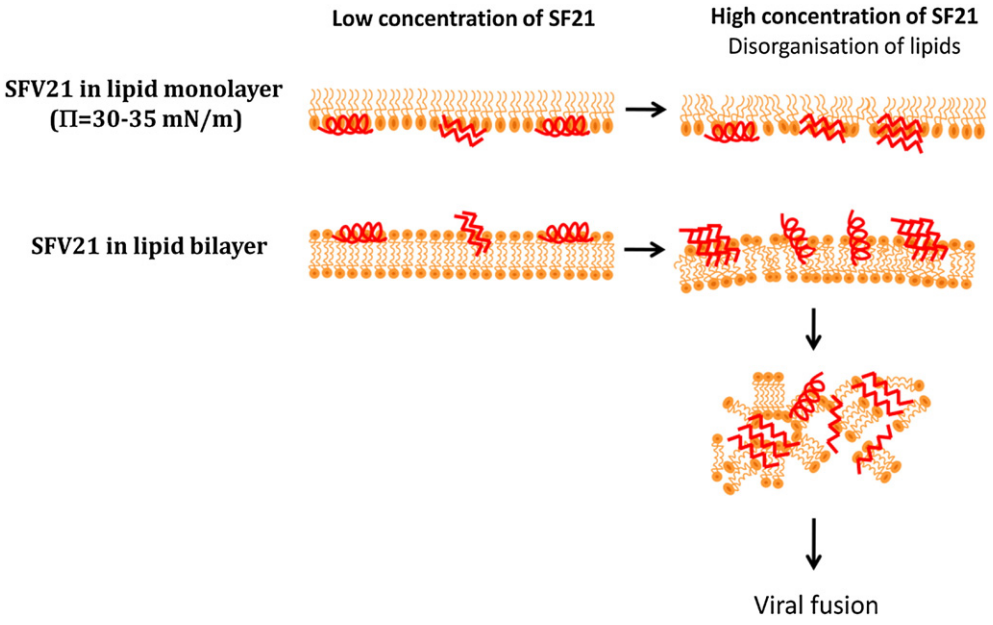

Fig. 7. Molecular cartoon of the SFV21 structure and orientation in the lipid mono/bi-layer as a function of the peptide concentration.

References

[1] W. Weissenhorn, A. Hinza, Y. Gaudin, Virus membrane fusion, FEBS Lett. 581 (2007) 2150–2155.
[2] M. Kielian, F.A. Rey, Virus membrane-fusion proteins: more than one way to make a hairpin, Nat. Rev. Microbiol. 4 (2006) 67–76.
[3] M. Kielian, Class II virus membrane fusion proteins, Virology 344 (2006) 38–47, http://dx.doi.org/10.1016/j.virol.2005.09.036.
[4] T.S. Jardetzky, R.A. Lamb, A class act, Nature 427 (2004) 307–308.
[5] M.-C. Vaney, F.A. Rey, Class II enveloped viruses, Cell. Microbiol. 13 (2011) 1451–1459.
[6] J.M. White, Viral and cellular membrane fusion proteins, Annu. Rev. Physiol. 50 (1990) 675–697.
[7] S.C. Harrison, Mechanism of membrane fusion by viral envelop proteins, Adv. Virus Res. 64 (2005) 231–261.
[8] S.C. Harrison, Viral membrane fusion, Virology 479-480 (2015) 498–507.
[9] A.E. Smith, A. Helenius, How viruses enter animal cells? Science 304 (2004) 237–242.
[10] S.B. Sieczkarski, G.R. Whittaker, Viral entry, Curr. Top. Microbiol. Immunol. 285 (2005) 1–23.
[11] J. Nieva, Are fusion peptides a good model to study viral cell fusion? Biochim. Biophys. Acta Biomembr. 1614 (2003) 104–115, http://dx.doi.org/10.1016/S0005-2736(03)00168-8.
[12] S. Castano, B. Desbat, Structure and orientation study of fusion peptide FP23 of gp41 from HIV-1 alone or inserted into various lipid membrane models (mono-, bi- and multibi-layers) by FT-IR spectroscopies and Brewster angle microscopy, Biochim. Biophys. Acta Biomembr. 1715 (2005) 81–95.
[13] V. Buzón, E. Padrós, J. Cladera, Interaction of fusion peptides from HIV gp41 with membranes: a time-resolved membrane binding, lipid mixing, and structural study, Biochemistry (Mosc) 44 (2005) 13354–13364.
[14] Y. Li, L.K. Tamm, Structure and plasticity of the human immunodeficiency virus gp41 fusion domain in lipid micelles and bilayers, Biophys. J. 93 (2007) 867–886.
[15] B. Barz, W. T. C., I. Kosztina, Membrane curvature and surface area per lipid affect the conformation and oligomeric state of HIV-1 fusion peptide: a combined FTIR and MD simulation study, Biochim. Biophys. Acta Biomembr. 1776 (2007) 945–953.
[16] S. Tristram-Nagle, R. Chan, E. Kooijman, P. Uppamoochikkal, W. Qiang, D.P. Weliky, J.F. Nagle, HIV fusion peptide penetrates, disorders, and softens T-cell membrane mimics, J. Mol. Biol. 402 (2010) 139–163.
[17] C.M. Gabrys, W. Qiang, Y. Sun, L. Xie, S.D. Schmick, D.P. Weliky, Solid-state nuclear magnetic resonance measurements of HIV fusion peptide (CO)-C-13 to lipid P-31 proximities support similar partially inserted membrane locations of the alpha helical and beta sheet peptide structures, J. Phys. Chem. A 117 (2013) 9848–9859.
[18] P. Shchelokovskyy, S. Tristram-Nagle, D. Dimova, Effect of the HIV-1 fusion peptide on the mechanical properties and leaflet coupling of lipid bilayers, New J. Phys. 13 (2011).
[19] C. Shoch, R. Blumenthal, Role of the fusion peptide sequence in initial-stages of influenza hemagglutinin-induced cell-fusion, J. Biol. Chem. 268 (1993) 9267–9274.
[20] R. Epand, R. Epand, Relationship between the infectivity of influenza-virus and the ability of its fusion peptide to perturb bilayers, Biochem. Biophys. Res. Commun. 202 (1994) 1420–1425.
[21] K.J. Cross, W.A. Langley, R.J. Russell, J.J. Skehel, D.A. Steinhauer, Composition and functions of the influenza fusion peptide, Protein Pept. Lett. 16 (2009) 766–778.
[22] J.L. Lorieau, J.M. Louis, C.D. Schwieters, A. Bax, pH-triggered, activated-state conformations of the influenza hemagglutinin fusion peptide revealed by NMR, Proc. Natl. Acad. Sci. U. S. A. 109 (2012) 19994–19999.
[23] B. Sainz, J. Rausch, W. Gallaher, R. Garry, W. Wimley, Identification and characterization of the putative fusion peptide of the severe acute respiratory syndrome-associated coronavirus spike protein, J. Virol. 79 (2005) 7195–7206.
[24] J. Guillen, R.F.M. De Almeida, M. Prieto, J. Villalain, Interaction of a peptide corresponding to the loop domain of the S2 SARS-CoV virus protein with model membranes, Mol. Membr. Biol. 26 (2009) 236–248.
[25] F.M. Ruiz-Argüello, M. Begoña Goñi, F.B. Pereira, J.L. Nieva, Phosphatidylinositol-dependent membrane fusion induced by a putative fusogenic sequence of Ebola virus, J. Virol. 72 (1998) 1775–1781.
[26] M.S. Freitas, L.P. Gaspar, M. Lorenzoni, F.C.L. Almeida, L.W. Tinoco, M.S. Almeida, L.F. Maia, L. Degrève, A.P. Valente, J.L. Silva, Structure of the Ebola fusion peptide in a membrane-mimetic environment and the interaction with lipid rafts, J. Biol. Chem. 282 (2007) 27306–27314, http://dx.doi.org/10.1074/jbc.M611864200.
[27] A. Agopian, S. Castano, Structure and orientation study of Ebola fusion peptide inserted in lipid membrane models, Biochim. Biophys. Acta Biomembr. 1838 (2014) 117–126.
[28] H. Yao, M. Hong, Membrane-dependent conformation, dynamics, and lipid interactions of the fusion peptide of the paramyxovirus PIV5 from solid-state NMR, J. Mol. Biol. 425 (2013) 563–576.
[29] H. Yao, M. Hong, Conformation and lipid interaction of the fusion peptide of the paramyxovirus PIV5 in anionic and negative-curvature membranes from solid-state NMR, J. Am. Chem. Soc. 136 (2014) 2611–2624, http://dx.doi.org/10.1021/ja4121956.
[30] M.N. Melo, F.J.R. Sousa, F.A. Carneiro, M.A.R.B. Castanho, A.P. Valente, F.C.L. Almeida, A.T. Da Poian, R. Mohana-Borges, Interaction of the Dengue virus fusion peptide with membranes assessed by NMR: the essential role of the envelope protein Trp101 for membrane fusion, J. Mol. Biol. 392 (2009) 736–746.
[31] H. Mohanram, A. Nip, P.N. Domadia, A. Bhunia, S. Bhattacharjya, et al., Biochemistry (Mosc) 51 (2012) 7863–7872, http://dx.doi.org/10.1021/bi300901f.
[32] J. Lescar, A. Roussel, M.W. Wien, J. Navaza, S.D. Fuller, G. Wengler, F.A. Rey, The fusion glycoprotein shell of Semliki Forest virus: an icosahedral assembly primed for fusogenic activation at endosomal pH, Cell 105 (2001) 137–148.
[33] D.L. Gibbons, A. Ahn, M. Liao, L. Hammar, R.H. Cheng, M. Kielian, Multistep regulation of membrane insertion of the fusion peptide of Semliki Forest virus multistep regulation of membrane insertion of the fusion peptide of Semliki Forest virus, J. Virol. 78 (2004) 3312–3318, http://dx.doi.org/10.1128/JVI.78.7.3312.
[34] A. Roussel, J. Lescar, M.-C. Vaney, G. Wengler, G. Wengler, F.a. Rey, Structure and interactions at the viral surface of the envelope protein E1 of Semliki Forest virus, Struct. Lond. Engl. 14 (2006) 75–86, http://dx.doi.org/10.1016/j.str.2005.09.014 (1993).
[35] H. Garoff, A.M. Frischauf, K. Simons, H. Lehrach, H. Delius, Nucleotide sequence of cDNA coding for Semliki Forest virus membrane glycoproteins, Nature 288 (1980) 236–241.
[36] P. Levy-Mintz, M. Kielian, Mutagenesis of the putative fusion domain of the Semliki Forest virus spike protein, J. Virol. 65 (1991) 4292–4300.
[37] L. Hammar, S. Markarian, L. Haag, H. Lankinen, A. Salmi, R.H. Cheng, Prefusion rearrangements resulting in fusion peptide exposure in Semliki forest virus, J. Biol. Chem. 278 (2003) 7189–7198, http://dx.doi.org/10.1074/jbc.M206015200.
[38] S.G. Shome, M. Kielian, Differential roles of two conserved glycine residues in the fusion peptide of Semliki Forest virus, Virology 279 (2001) 146–160, http://dx.doi.org/10.1006/viro.2000.0688.
[39] D. Blaudez, T.T. Buffeteau, J.C. Cornut, B. Desbat, N. Escafre, M. Pezolet, J.M. Turlet, Polarization modulation FTIR spectroscopy at the air-water interface, Thin Solid Films 242 (1994) 146–150.
[40] E. Goormaghtigh, V. Cabiaux, J.M. Ruysschaert, Secondary structure and dosage of soluble and membrane proteins by attenuated total reflection Fourier-transform infrared spectroscopy on hydrated films, Eur. J. Biochem. 193 (1990) 409–420.
[41] E. Goormaghtigh, V. Cabiaux, J.M. Ruysschaert, Determination of soluble and membrane protein structure by Fourier transform infrared spectroscopy. III. Secondary structures, Subcell. Biochem. 23 (1994) 405–450.
[42] E. Goormaghtigh, V. Raussens, J.M. Ruysschaert, Attenuated total reflection infrared spectroscopy of proteins and lipids in biological membranes, Biochim. Biophys. Acta 1422 (1999) 105–185.
[43] R.M.A. Azzam, N.M. Bashara, Ellipsometry and Polarized Light, North-Holl, Amsterdam, 1977.
[44] Z. Fezoua-Boubegtiten, B. Desbat, A. Brisson, S. Lecomte, Determination of molecular groups involved in the interaction of annexin A5 with lipid membrane models at the air-water interface, Biochim. Biophys. Acta. 1798 (2010) 1204–1211.
[45] D. Blaudez, F. Boucher, T. Buffeteau, B. Desbat, M. Grandbois, S. C., Anisotropic optical constants of bacteriorhodopsin in the mid-infrared: consequence on the determination of alpha-helix orientation, Appl. Spectrosc. 53 (1999) 1299–1304.
[46] S. Castano, D. Blaudez, B. Desbat, J. Dufourcq, H. Wróblewski, Secondary structure of spiralin in solution, at the air/water interface, and in interaction with lipid monolayers, Biochim. Biophys. Acta 1562 (2002) 45–56.
[47] D. Ducharme, J.J. Max, C. Salesse, R.M. Leblanc, Ellipsometric study of the physical states of phosphatidylcholines at the air-water interface, J. Phys. Chem. 94 (1990) 1925–1932.
[48] J. Saccani, S. Castano, B. Desbat, D. Blaudez, A phospholipid bilayer supported under a polymerized Langmuir film, Biophys. J. 85 (2003) 3781–3787.
[49] W.K. Surewicz, H.H. Mantsch, D. Chapman, Determination of protein secondary structure by Fourier transform infrared spectroscopy: a critical assessment, Biochemistry (Mosc) 32 (1993) 389–394.
[50] P.I. Haris, D. Chapman, Does Fourier-transform infrared spectroscopy provide useful information on protein structures? Trends Biochem. Sci. 17 (1992) 328–333.
[51] S. Castano, B. Desbat, M. Laguerre, J. Dufourcq, Structure, orientation and affinity for interfaces and lipids of ideally amphipathic lytic LiKj(i = 2j) peptides, Biochim. Biophys. Acta 1416 (1999) 176–194.
[52] S. Castano, B. Desbat, J. Dufourcq, Ideally amphipathic beta-sheeted peptides at interfaces : structure , orientation , a ¤ nities for lipids and hemolytic activity of (KL)mK peptides, Biochim. Biophys. Acta 1463 (2000) 65–80.
[53] G. van Meer, D. Voelker, G. Feigenson, Membrane lipids: where they are and how they behave, Nat. Rev. Mol. Cell Biol. 9 (2008) 112–124.
[54] J. Minones Jr., J. Minomes, O. Conde, P. Dynarowicz-Latka, Interactions between membrane sterols and phospholipids in model mammalian and fungi cellular membranes. A Langmuir monolayer study, Biophys. Chem. 140 (2009) 69–77.
[55] H.H. Mantsch, R.N. McElhaney, Phospholipid phase transitions in model and biological membranes as studied by infrared spectroscopy, Chem. Phys. Lipids 57 (1991) 213–226.
[56] D. Blaudez, S. Castano, B. Desbat, PM-IRRAS at liquid interfaces, in: C.M. Pradier, Y.J. Chabal (Eds.), Biointerface Charact, Adv. IR Spectrosc., Elsevier 2011, pp. 27–56.
[57] D. Blaudez, J. Turlet, J. Dufourcq, D. Bard, T. Buffeteau, B. Desbat, Investigations at the air/water interface using polarization modulation IR spectroscopy, Faraday Trans. 92 (1996) 525–530.
[58] M.W. Rooney, Y. Lange, J.W. Kauffman, Acyl chain organization and protein secondary structure in cholesterol-modified erythrocyte membranes, J. Biol. Chem. 259 (1984) 8281–8285.
[59] D.G. Cameron, H.L. Casal, H.H. Mantsch, Characterization of the pretransition in 1,2-dipalmitoyl-sn-glycero-3-phosphocholine by Fourier transform infrared spectroscopy, Biochemistry (Mosc) 19 (1980) 3665–3672.
[60] I.M. Asher, I.W. Levin, Effects of temperature and molecular interactions on the vibrational infrared spectra of phospholipid vesicles, Biochim. Biophys. Acta 468 (1977) 63–72.
[61] D. Gidalevitz, Z. Huang, S.A. Rice, Protein folding at the air–water interface studied with x-ray reflectivity, Proc. Natl. Acad. Sci. U. S. A. 96 (1999) 2608–2611.

[62] D.F. Chessman, J.T. Davies, Physicochemical and biological aspects of proteins at interfaces, Adv. Protein Chem. 9 (1954) 439–501.
[63] A. Linetti, A. Fratangeli, P. Rosa, Cholesterol reduction impairs exocytosis of synaptic vesicles, J. Cell Sci. 123 (2010) 595–605.
[64] X. Sun, G.R. Whittaker, Role for influenza virus envelope cholesterol in virus entry and infection, J. Virol. (2003) 12543–12551.
[65] D.-A.L. Lai, A.E. Moorthy, Y. Li, L.K. Tamm, Fusion activity of HIV gp41 fusion domain is related to its secondary structure and depth of membrane insertion in a cholesterol dependent, J. Mol. Biol. 418 (2012) 3–15.
[66] S.-T. Yang, V. Kiessling, J.A. Simmons, J.M. White, L.K. Tamm, HIV gp41–mediated membrane fusion occurs at edges of cholesterol-rich lipid domains, Nat. Chem. Biol. 11 (2015) 424–431.
[67] B. Apellaniz, J.L. Nieva, Fusion-competent state induced by a C-terminal HIV-1 fusion peptide in cholesterol-rich membranes, Biochim. Biophys. Acta Biomembr. 184 (2015) 1014–1022.
[68] G. Vitiello, G. Fragneto, A.A. Petruk, A. Falanga, S. Galdiero, A.-M. D'Ursi, A. Merlino, G. D'Errico, Cholesterol modulates the fusogenic activity of a membranotropic domain of the FIV glycoprotein gp36, Soft Matter 9 (2013) 6442–6456.
[69] G. Vitiello, A.A. Falanga, A. Petruk, G. Merlino, L. Fragneto, S. Paduano, G. Galdiero, D'Errico, Fusion of raft-like lipid bilayers operated by a membranotropic domain of the HSV-type I glycoprotein gH occurs through a cholesterol-dependent mechanism, Soft Matter 11 (2015) 3003–3016.
[70] J.E. Voss, M.C. Vaney, S. Duquerroy, C. Vonrhein, C. Girard-Blanc, E. Crublet, A. Thompson, G. Bricogne, F.A. Rey, Glycoprotein organization of chikungunya virus particles revealed by X-ray crystallography, Nature 468 (2010) 709–712.
[71] W. Yassine, N. Taib, S. Federman, A. Milochau, S. Castano, W. Sbi, C. Manigand, M. Laguerre, B. Desbat, R. Oda, J. Lang, Reversible transition between alpha-helix and beta-sheet conformation of a transmembrane domain, Biochim. Biophys. Acta 1788 (2009) 1722–1730, http://dx.doi.org/10.1016/j.bbamem.2009.05.014.
[72] K. Kliger, A. Aharoni, D. Rapaport, P. Jones, R. Blumenthal, Y. Shai, Fusion peptides derived from the HIV type 1 glycoprotein 41 associate within phospholipid membranes and inhibit cell–cell fusion. Structure –function study, J. Biol. Chem. 272 (1997) 13496–13505.
[73] Y. Yang, M. Gabrys, D.P. Weliky, Solid-state NMR evidence for an extended hstrand conformation of the membrane bound HIV-1 fusion peptide, Biochemistry (Mosc) 40 (2001) 8126–8137.
[74] D. Rapaport, Y. Shai, Interaction of fluorescently labeled analogues of the amino-terminal fusion peptide of Sendai virus with phospholipid membranes, J. Biol. Chem. 26 (1994) 15124–15131.
[75] H.-P.K. Kinnunen, J.M. Holopainen, Mechanisms of initiation of membrane fusion: role of lipids, Biosci. Rep. 20 (2000) 465–482.
[76] D.J. Schibli, W. Weissenhorn, Class I and class II viral fusion protein structures reveal similar principles in membrane fusion (Review), Mol. Membr. Biol. 21 (2004) 361–371.